

Correlation Strength and Particle-Hole Asymmetry in High- T_c Cuprates: a Dynamical Mean Field Study of the Three-Band Copper-Oxide Model

Luca de' Medici¹, Xin Wang², Massimo Capone³, and Andrew J. Millis²

⁽¹⁾*Department of Physics and Center for Materials Theory,*

Rutgers the State University of NJ, 136 Frelinghuysen Road, Piscataway, NJ 08854

⁽²⁾*Department of Physics, Columbia University, 538 W. 120th Street, New York, NY 10027 USA*

⁽³⁾*SMC, CNR-INFM, and Dipartimento di Fisica,*

Universit di Roma "La Sapienza", Piazzale A. Moro 2, I-00185, Rome, Italy and ISC-CNR, Via dei Taurini 18, I-00185, Rome, Italy

(Dated: March 15, 2019)

The three-band model relevant for high temperature copper-oxide superconductors is solved using single-site dynamical mean field theory. The calculation includes the physics of "Zhang-Rice singlets". The metal/charge-transfer-insulator phase diagram, spectral function, optical conductivity and mass enhancement are computed. The "mid-infrared" optical spectral weight induced by doping is found to be comparable for electron and hole-doped compounds; however the quasiparticle mass enhancement is larger for hole than for electron-doped compounds.

PACS numbers:

Although more than two decades have passed since the discovery of high temperature superconductivity in $La_{2-x}Sr_xCuO_4$ and related compounds, many aspects of the high- T_c phenomenon remain mysterious. High T_c materials are created by doping insulating parent compounds, but doping with electrons and with holes leads to different behavior. The hole-doped materials exhibit superconductivity over relatively wide doping regimes, and for temperatures which can be much greater than 100K while the electron-doped materials exhibit superconductivity only at relatively low temperatures (less than 25K) and only in a very narrow region of composition. Conversely, magnetism plays a much more obvious role in the phase diagram of electron-doped materials than in the phase diagram of the hole-doped materials.

The observed particle-hole asymmetry in the properties of high- T_c cuprates presumably arises because the materials are "charge-transfer insulators" [1]. As noted in ref [1], although the strong correlations are associated with the Cu- d -orbitals, oxygen $2p$ levels are important. If the O_{2p} states are close to or higher-lying in energy than the Cu d^{10} states the stoichiometric compound is metallic while if the Cu d^{10} states lie significantly higher the stoichiometric compound is insulating and while doped electrons reside mainly on the Cu, doped holes go on the O, but may be bound to Cu spins [2, 3] creating "Zhang-Rice singlets".

Quantifying these ideas requires solving an electronic structure problem with multiple scales, including a correlation energy on the Cu site $\sim 8 - 10eV$, a Cu-O energy level difference of $2 - 4eV$ [4, 5], and a Cu-O hybridization $\sim 1.6eV$ [6]. In this paper we use single-site Dynamical Mean-Field Theory (DMFT) with new or newly improved Exact Diagonalization (ED)[7, 8] and Continuous-Time Quantum Monte Carlo (CT-QMC)[9] impurity solvers to develop a comprehensive theoretical picture of the electronic structure and optical con-

ductivity of undoped and doped materials across the charge-transfer-insulator to charge-transfer metal phase diagram.

Our work is related to previous work of Georges *et al.*[10], but modern developments in computers and solvers mean that we are able to obtain much more information, and to more recent work of Macridin *et al.* [11] who used the Dynamical Cluster Approximation on a four site cluster to study momentum dependence and the onset of superconductivity. We focus on the spectral functions over a wider energy range, on the optical conductivity, and on exploring both the metallic and insulating regimes of the phase diagram. We analyse the canonical two dimensional "three-band" Hamiltonian [2, 12] retaining the Cu $d_{x^2-y^2}$ and O $2p_\sigma$ orbitals (whose momentum (p) components are created by the operators $d_{p\sigma}^\dagger, p_{x,p\sigma}^\dagger, p_{y,p\sigma}^\dagger$). The Hamiltonian is $H = H_{3band} + H_{int}$, with

$$H_{3band} = \sum_{p\sigma} (d_{p\sigma}^\dagger \ p_{x,p\sigma}^\dagger \ p_{y,p\sigma}^\dagger) H_p \begin{pmatrix} d_{p\sigma} \\ p_{x,p\sigma} \\ p_{y,p\sigma} \end{pmatrix}, \quad (1)$$

$$H_p = \begin{pmatrix} \varepsilon_d & 2it_{pd} \sin \frac{p_x}{2} & 2it_{pd} \sin \frac{p_y}{2} \\ -2it_{pd} \sin \frac{p_x}{2} & \varepsilon_p & 0 \\ -2it_{pd} \sin \frac{p_y}{2} & 0 & \varepsilon_p \end{pmatrix}, \quad (2)$$

and $H_{int} = U \sum_i n_{d\uparrow} n_{d\downarrow}$. We neglect oxygen-oxygen hopping; this is not important for our considerations. Because only the Cu site is interacting, we may integrate out the oxygen band to obtain an effective one-orbital model, which we solve in the single-site DMFT [13] using methods described in the literature [7, 8, 9].

Fig. 1 shows the boundary between metallic and insulating solutions, calculated for one hole per CuO₂ unit as a function of interaction strength U and Cu-O energy level splitting $\Delta (= \varepsilon_p - \varepsilon_d)$ in the paramagnetic

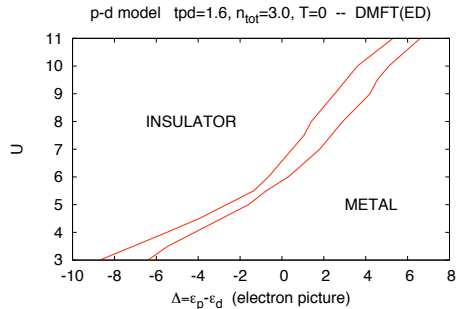


FIG. 1: Metal-insulator phase diagram in phase space of interaction U and $p-d$ level splitting Δ for one hole per CuO_2 unit. In the region between the two lines metallic and insulating solutions coexist.

phase. The phase diagram is consistent with the arguments of Zaanen, Sawatzky and Allen [1]: at fixed large U the metal-insulator transition is of the charge-transfer type, driven by variation of the Cu-O energy level difference Δ . The low-energy physics arises from the $\text{Cu } d^{10}$ (energy $\sim \varepsilon_d + U$) and O_{2p} (energy $\varepsilon_p = \varepsilon_d + \Delta$) states. If these are nearby in energy (large Δ) the model is metallic even at the commensurate density of 1 hole per site, while if the O states lie too low in energy (small Δ) the model is insulating. As in the single-site DMFT of the one-band Hubbard model [13] a coexistence region is observed where both metallic and insulating solutions exist. We define the insulating boundary of the coexistence region at fixed large U to be Δ_{c2} and the metallic boundary to be Δ_{c1} . The phase diagram is obtained at $T = 0$ using the ED solver; the results were verified using CT-QMC by scanning Δ at selected U values. We find almost perfect agreement for Δ_{c1} ; the CT-QMC calculation yield a larger Δ_{c2} ; the difference arises from the strong T -dependence of the phase boundary [13].

Fig. 2 presents the total many body density of states (electron removal spectrum for energy < 0 and electron addition spectrum for energy > 0) as well as the projections onto the Cu- d and O- $2p_\sigma$ states. We choose interaction $U = 9\text{eV}$ and $\Delta = 2\text{eV} \lesssim \Delta_{c2}$ (lower panel) and $4\text{eV} \approx \Delta_{c1}$ (upper panel). The zero of energy is the chemical potential. In the undoped insulating case (lower panel, middle graph) a gap is evident at the chemical potential. At lowest energy (binding energy $\sim 11\text{eV}$) a peak is seen, of mainly d -character. This peak corresponds to removing one electron and leaving the Cu in the d^8 state. At binding energy $\varepsilon \sim -6 \sim -9\text{eV}$ a mainly oxygen-like band is seen. The very sharp peak corresponds to the non-bonding oxygen state; the broad structure of mainly oxygen character lying below this may be thought of as the “bonding” linear combination of Cu and O states, pushed down below the non-bonding

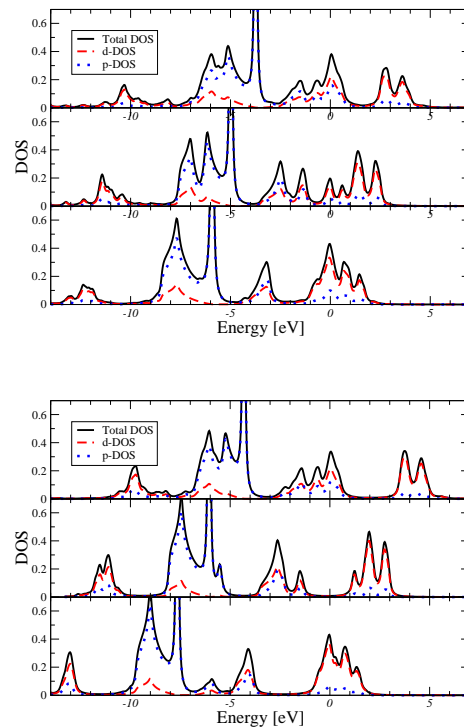


FIG. 2: Electron spectral function per spin (negative frequency: removal spectrum; positive frequency: addition spectrum) (solid lines) and projections onto d (dashed; red online) and p (dotted line; blue online) states for three-band model with $U = 9\text{eV}$ and $\Delta = 4\text{eV}$ (upper panels) and $\Delta = 2\text{eV}$ (lower panels). Upper graphs: 0.15 hole doping ($\Delta = 4\text{eV}$: $\varepsilon_d = -7.7\text{eV}$, $\varepsilon_p = -3.7\text{eV}$; $\Delta = 2\text{eV}$, $\varepsilon_d = -6.3\text{eV}$, $\varepsilon_p = -4.3\text{eV}$) middle graphs: undoped ($\Delta = 4\text{eV}$, $\varepsilon_d = -10.8\text{eV}$, $\varepsilon_p = -6.8\text{eV}$ and $\Delta = 2\text{eV}$, $\varepsilon_d = -7.0\text{eV}$, $\varepsilon_p = -5.0\text{eV}$). Lower graphs: 0.15 electron doping ($\Delta = 4\text{eV}$, $\varepsilon_d = -9.9\text{eV}$, $\varepsilon_p = -5.9\text{eV}$; $\Delta = 2\text{eV}$; $\varepsilon_d = -9.6\text{eV}$, $\varepsilon_p = -7.6\text{eV}$).

O level by hybridization to the $\text{Cu } d$ level. We identify the structure of mixed Cu-O character at binding energies in the range $\varepsilon \sim 2 - 5\text{eV}$ as the Zhang-Rice singlet states. This identification is confirmed by calculations (not shown here) in which the Cu orbital is forced to be fully spin polarized; these reveal that these states correspond to holes with the same spin as the deep-lying removal state. The states in the electron addition spectrum are mainly of $\text{Cu } d^{10}$ character, and play the role of the upper Hubbard band.

The densities of states for the undoped metallic case (upper panel, middle graph) are broadly similar to those of the insulating case, except that the d^{10} states are a bit lower in energy enabling states to appear at the chemical potential. The deep-lying copper level and Zhang-Rice singlet band remain at almost the same position with respect to the Fermi level; the increase in Δ shifts the non-bonding O states closer to the Fermi level.

Upon doping, two changes occur. First, the chemical potential moves into the Zhang-Rice band (hole doping) or the upper Hubbard band (electron doping). The asso-

	$\Delta = 4eV$			$\Delta = 2eV$		
dop	-0.15	0.00	0.15	-0.15	0.00	0.15
d^s	0.33	0.45	0.31	0.50	0.54	0.37
Z-R	1.2	0.76	0.52	1.1	0.83	0.68
UHB	0.82	1.0	1.5	0.83	1.03	1.34

TABLE I: Integrated density of states (both spins) for the d^s (lowest-lying), “Zhang-Rice” (ZR) and “Upper Hubbard Band” (UHB) spectral features discussed in the text for $U = 9eV$, $\Delta = 4eV$ (metal at half filling) and $\Delta = 2eV$ (insulator at half filling) at dopings indicated.

ciated changes in chemical potential are substantial: the Fermi level, measured relative to the non-bonding oxygen band, shifts by almost $2eV$. Second, as can be seen by inspection of the figures, the relative strengths of the different spectral features evolve. Table I quantifies this, showing the total number of states in the d^s , Zhang-Rice and upper Hubbard band features for the different dopings and the two Δ -values. The issue of the number of states created by doping has received some attention in the literature as a signature of “Mottness” [14]. We find that the changes in the spectrum do not have a universal doping or interaction-strength dependence; however in the “charge-transfer insulating” regime $\Delta \lesssim \Delta_{c2}$ each doped hole adds about two states to the Zhang-Rice band and one to the upper Hubbard band, while doping with electrons does essentially the opposite. The dynamical mean field method provides spectroscopic information on single-particle and two-particle response functions. The upper panel of Fig. 3 shows the fermi-surface mass renormalization factor $-\partial\Sigma/\partial|\omega_{\omega \rightarrow 0}$ estimated from the values of $Im\Sigma(i\omega_n)$ at the lowest two Matsubara points of the ED calculation. At very low doping the estimate becomes unreliable because the (very small) fermi liquid scale is not easily resolved so we do not present results. For $\Delta \sim \Delta_{c2}$ a striking particle-hole asymmetry is evident, with the renormalization factor being rather larger for the hole-doped than for the electron-doped materials. The lower panel of Fig. 3 shows the self energy over a wider range, for the “metallic” case $\Delta = 4$ and doping ± 0.18 . The good agreement between ED and CT-QMC calculations confirms the reliability of our results. One sees $\sim 40\%$ differences at higher frequencies, larger than the difference ($\sim 10\%$) in renormalization factor.

We have calculated the optical conductivity using the Kubo formula and the minimal coupling ansatz $\vec{p} \rightarrow \vec{p} - \vec{A}$. The dissipative part of the conductivity is then

$$\sigma(\Omega) = \int_{-\infty}^{\infty} \frac{d\omega}{\pi} \int \frac{d^2p}{(2\pi)^2} \frac{f(\omega) - f(\omega + \Omega)}{\Omega} \quad (3)$$

$$\times Tr [j_{3band}(p)\mathbf{A}(\omega + \Omega, p)j_{3band}(p)\mathbf{A}(\omega, p)]$$

where the spectral function $\mathbf{A}(\omega, p) = \frac{i}{2} (\mathbf{G}(\omega, \Sigma(\omega + i\epsilon, p)) - \mathbf{G}(\omega, \Sigma(\omega - i\epsilon, p)))$ and the matrix Green function \mathbf{G} at frequency z is

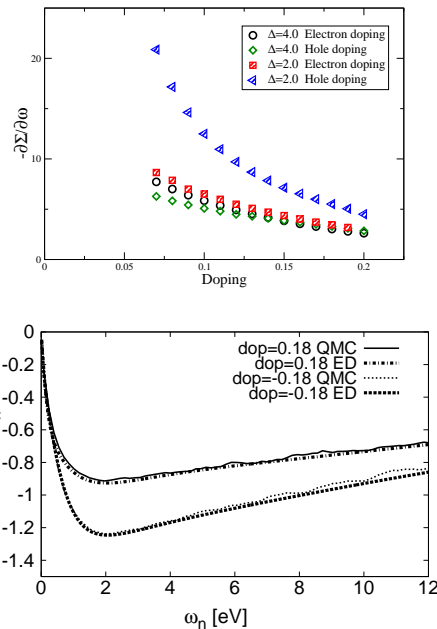


FIG. 3: Upper panel: doping dependence of fermi surface mass renormalization factor $-\partial\Sigma/\partial\omega|_{\omega \rightarrow 0}$ estimated from lowest two Matsubara points obtained from ED calculations. Lower panel: comparison of CT-QMC and ED results for $\Delta = 4eV \gtrsim \Delta_{c1}$ and dopings indicated

$\mathbf{G}(z, p) = (z\mathbf{1} - \Sigma(z) - H_{3band})^{-1}$. The current operator $j = \delta H/\delta p_x$ is

$$j_{3band} = \begin{pmatrix} 0 & -it_{pd} \cos \frac{p_x}{2} & 0 \\ it_{pd} \cos \frac{p_x}{2} & 0 & 0 \\ 0 & 0 & 0 \end{pmatrix} \quad (4)$$

We verified the prefactor by comparison of the weight in the Drude peak to the fermi surface average of the renormalized fermi velocity

The dotted lines in Fig 4 show the conductivity calculated for the undoped case. The strong absorption in the range $6eV < \Omega < 9eV$ ($\Delta \sim \Delta_{c1}$ (metallic)) or $7eV < \Omega < 10eV$ ($\Delta \sim \Delta_{c2}$ (insulating)) cases arises from transitions from non-bonding and bonding oxygen states to the upper Hubbard band. For $\Delta \sim \Delta_{c2}$ (lower panel) the weak absorption peaking at $\Omega \approx 4.5eV$ arises from transitions from the Zhang-Rice (or lower Hubbard) band to the upper Hubbard band, and is the analogue of the interband transition in the Mott insulating phase of the Hubbard model. For $\Delta \sim \Delta_{c1}$ the metallic nature of the half-filled state means that absorption persists down to low frequency. The magnitude and form of conductivity of the undoped case agree well with previous calculations for the one-band Hubbard model [15].

Electron or hole doping adds optical absorption strength (associated with motion of doped holes) at frequencies $\Omega \lesssim 2eV$. For both values of Δ the integrated absorption strength (up to $2eV$) is found to be comparable for electron and hole doping, despite the differences

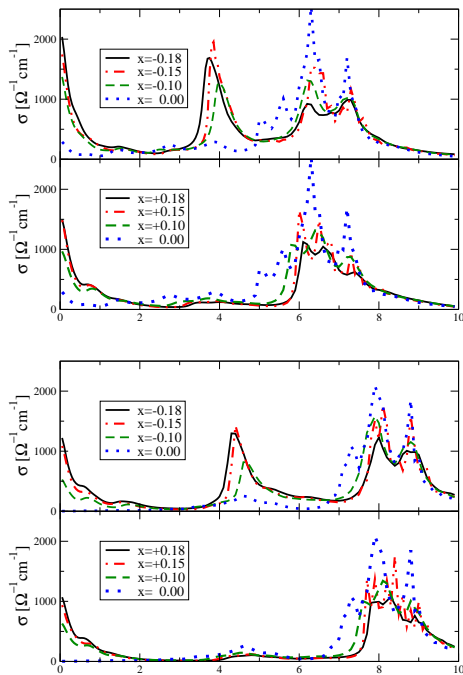


FIG. 4: Optical conductivity calculated for three-band model with $U = 9eV$, $\Delta = 4eV$ (upper panels), and $\Delta = 2eV$ (lower panels) for dopings indicated. Other parameters as in Fig. 2.

in self energy displayed in Fig 3. In this frequency range, the optical matrix element is proportional to the fermi velocity which depends on the renormalized $Cu-O$ energy difference set by the parameter $\Delta - Re\Sigma(\omega)$. The shifts in $Re\Sigma$ as the chemical potential is tuned from hole to electron doping leads (especially for $\Delta \lesssim \Delta_{c2}$) to a bare fermi velocity which is $\sim 40\%$ or more larger on the hole-doped side than on the electron-doped side so the change in optical matrix element compensates for the difference in mass enhancement. One of us previously argued [17] that the experimentally observed similarity in low frequency optical absorption between electron and hole-doped materials implied that the correlation strength was about the same for two systems; we see that this argument must be treated with caution.

The more striking change is that hole-doping but not electron doping activates a strong transition (at about $4eV$ in our calculations) between the non-bonding oxygen band and the near-fermi-surface states which increases in strength and moves down in energy as doping is increased. This feature is not observed experimentally; indeed a comparison of figs 7 and 8 of Ref [16] shows that in the range $\Omega \sim 4eV$ the optical absorption in electron doped compounds is slightly larger than in hole-doped compounds. Further experimental and theoretical investigation of this issue is important.

In conclusion, we have used dynamical mean field methods to solve the three band model believed to be

relevant to the copper-oxide materials. The method reproduces the characteristic features of the spectrum and reveals (especially for parameters in the "charge transfer insulator" regime) a striking particle-hole asymmetry both in the quasiparticle band structure (bare hole velocity larger than bare electron velocity) and in the renormalization strength, with the two effects to a large degree cancelling in the low frequency optics.

As this manuscript was being completed we became aware of closely related work of Weber, Haule and Kotliar [18] who studied carefully one parameter set, obtained from LDA and corresponding to Δ slightly smaller than Δ_{c2} . Where there is overlap the conclusions are similar; differences of detail which will be discussed elsewhere.

Acknowledgements This collaboration was begun with support from the Columbia/Polytechnique/Science Po/Sorbonne Alliance program. AJM and XW are supported by NSF-DMR-0705847 and MC by MIUR PRIN 2005, Prot. 200522492 and LdM by the Rutgers Center for Materials Theory and NSF DMR 0528969.

-
- [1] J. Zaanen, G. Sawatzky, and J. Allen, Phys. Rev. Lett. **55** 418 (1985).
 - [2] V. Emery, Phys. Rev. Lett. **58** 2794 (1987).
 - [3] F. C. Zhang and T. M. Rice, Phys. Rev. B **37** 3659 (1988).
 - [4] F. Mila, F. C. Zhang, and T. M. Rice, Physica C **153-155** 1221 (1988).
 - [5] M. A. van Veenendaal, G. A. Sawatzky, and W. A. Groen, Phys. Rev. B **49** 1407 (1994).
 - [6] O. K. Andersen, A. I. Liechtenstein, O. Jepsen, and F. Paulsen, J. Phys. Chem. Solids **56**, 1573 (1995).
 - [7] M. Caffarel and W. Krauth, Phys. Rev. Lett. **72**, 1545 (1994).
 - [8] M. Capone, M. Civelli, S. S. Kancharla, C. Castellani, and G. Kotliar, Phys. Rev. B **69**, 195105 (2004).
 - [9] P. Werner, A. Comanac, L. de' Medici, M. Troyer, and A. J. Millis, Phys. Rev. Lett. **97**, 07640/1-45 (2006).
 - [10] A. Georges, B. G. Kotliar, and W. Krauth, Z. Phys. B **92** 313 (1993).
 - [11] A. Macridin, M. Jarrell, Th. Maier, and G. Sawatzky, Phys. Rev B **71** 134527 (2005).
 - [12] C. M. Varma, S. Schmitt-Rink, and E. Abrahams, Sol. St. Comm. **62** 681 (1987).
 - [13] A. Georges, B. G. Kotliar, W. Krauth, and M. Rozenberg, Rev. Mod. Phys **68** 13 (1996).
 - [14] M. B. J. Meinders, H. Eskes, and G. A. Sawatzky, Phys. Rev. B **48** 3916 (1993).
 - [15] A. Comanac, L. de' Medici, M. Capone, and A. J. Millis, Nat. Phys. **4** 287 (2008).
 - [16] S. Uchida, T. Ido, H. Takagi, T. Arima, Y. Tokura and S. Tajima, Phys. Rev. B **43** 7942 (1991).
 - [17] A. J. Millis, A. Zimmers, R. P. S. M. Lobo, N. Bontemps and C. C. Homes, Phys. Rev. B **72** 24517 (2005).
 - [18] C. Weber, K. Haule and G. Kotliar, arXiv0804.1512.